Acoustic generation of underwater cavities—Comparing modeled and measured acoustic signals generated by seismic air gun arrays

Babak Khodabandeloo[a] and Martin Landrø
Department of Geoscience and Petroleum, Norwegian University of Science and Technology (NTNU), NO-7491 Trondheim, Norway

Alfred Hanssen
Department of Geosciences, ARCEx, University of Tromsø, The Arctic University of Norway, NO-9037 Tromsø, Norway

(Received 18 November 2016; revised 15 February 2017; accepted 28 March 2017; published online 14 April 2017)

Underwater vapor cavities can be generated by acoustic stimulation. When the acoustic signals from several air guns are reflected from the sea surface, the pressure drop at some locations is sufficient for cavity growth and subsequent collapse. In this paper the generation of multiple water vapor cavities and their collapses are numerically modeled and the results are validated by comparing with field data from a seismic air gun array test. In a first modeling attempt where cavity interaction is neglected, a correspondence between measured and modeled data is found. Then, this correspondence is improved by assuming that the acoustic signal generated by the other cavities changes the hydrostatic pressure surrounding each cavity. This modeling can be used to estimate the amount and strength of high frequency signals generated by typical marine air gun arrays, given that a calibration step is performed prior to the modeling.

[http://dx.doi.org/10.1121/1.4979939]

[JFL] Pages: 2661–2672

I. INTRODUCTION

A. Background

Underwater man-made noise is recognized to have several adverse effects on aquatic animals and it is a worldwide problem (Southall *et al.*, 2008; Williams *et al.*, 2014). Such noise is mainly due to shipping, seismic surveys, military activities, and pile driving for offshore construction (Hildebrand, 2009). In marine seismic surveys, most common and widely used techniques utilize acoustic waves to image the Earths' subsurface. A majority of this type of survey is for hydrocarbon exploration. An active source radiates acoustic waves into the Earth and subsequently the subsurface structure is determined from measured reflected elastic waves using a large number of receivers. These receivers might be hydrophones organized in long cables that are towed behind the seismic vessel, or geophones that are deployed at the seabed. For seabed geophones, it is common today to measure the three spatial components of the displacement field (x, y, and z) and in addition to measure also the pressure component using a single hydrophone. This is known as four-component seismic, or 4C seismic.

On the other hand, acoustic waves that propagate in the water layer are crucial and a very effective sensory tool for marine mammals. These animals use sound for a variety of vital purposes such as foraging, social interactions, mating, navigation, and detecting predators (Wright *et al.*, 2007). Effects of the anthropogenic noise on marine fauna can be behavioral reactions (McCauley *et al.*, 2000), acoustic masking, prey effect, physiological effects (Nowacek *et al.*, 2007), and/or hearing impairment and threshold shifts (either temporarily or permanently) (Erbe and Farmer, 2000; Gordon *et al.*, 2003). Marine animals use different frequency ranges for communication and echolocation. Many species of toothed whales, one of two main groups of cetaceans, use 1–20 kHz for communication and 20–150 kHz for echolocation. The other group, baleen whales, uses lower frequencies ranging from 12 Hz to 8 kHz (Richardson *et al.*, 1995). To reduce the impact of noise on the marine mammals, it is reasonable to avoid or reduce overlap with their frequency ranges (Ketten, 2004). It should be noted that detailed knowledge of how and to what extent marine mammals exploit acoustic waves is still not fully explored.

Air gun arrays are the most common and efficient marine seismic source compared to other seismic sources such as marine vibrators and water-guns (Duren, 1988; Barger and Hamblen, 1980). Marine seismic acquisition is a major noise source in the marine environment and its impacts on aquatic life are therefore crucial to understand. Air guns produce loud impulsive bursts of underwater sound by a sudden release of high pressure air (typically 137 bar) which forms a rapidly expanding and contracting bubble (Caldwell and Dragoset, 2000). In practice instead of using one single air gun, several air guns with different volumes are used together which is referred to as an air gun array. The purpose of using many air guns is to increase the strength of the seismic source, to enhance the source signature, as well as to modify

[a]Electronic mail: babak.khodabandeloo@ntnu.no

directionality of the source to reduce the lateral directivity (Dragoset, 2000). Such arrays radiate acoustic waves that propagate through the water layer and into the subsurface beneath the seabed. Subsequently, seismic profiles for hydrocarbon exploration and scientific mapping of the Earths' crust are created from measured responses using receiver cables that are towed behind a seismic vessel or deployed at the seabed.

For seismic imaging, only low frequencies (less than 100 Hz) are required since they penetrate deeper into the Earth. However, there are also much higher frequencies generated by air gun arrays which do not benefit seismic imaging. Goold and Fish (1998) measured frequencies up to 22 kHz some kilometers away from a 2120 cubic inch air gun array. Using a broadband hydrophone, it was reported that air-gun arrays produce significant high frequencies up to 60 kHz (Landrø *et al.*, 2011) but much weaker than the signal recorded at seismic frequencies. These high frequencies emitted from air gun arrays overlap with the hearing curves of many cetacean species and may adversely affect them (Ketten, 2004, Landrø *et al.*, 2011). Despite some concerns about seismic air gun impact on marine life (NRC, 2003; Madsen *et al.*, 2006), they are still the dominant seismic source (Landrø and Amundsen, 2010; Weilgart, 2013). The main reason is that there is no better seismic source today and that the impact on marine life is considered low or minimal. Marine seismic vibrators were introduced a few years after the air gun and since then they have been in development. But they are still not a popular seismic source because of weak signal and practical issues related to operations. The radiated acoustic power is proportional to the square of the radiator size to the wavelength ratio (Norton and Karczub, 2003). Consequently they must be impractically large to radiate low frequency acoustic waves efficiently. Sources such as the Low level Acoustic Combustion Source (Askeland *et al.*, 2007), Tunable Organ Pipe (Morozov and Webb, 2007), Hydroacoustic Transduction (Bouyoucos, 1975), and low pressure air gun (Chelminski, 2015) may remain a future solution.

The interest to reduce the high frequency content generated by air gun arrays is increasing. An air gun silencer was tested for a 50 bar air gun and the experimental results showed that frequencies above 700 Hz were reduced by approximately 6 dB (Spence *et al.*, 2007). The drawbacks are the need for replacing acoustically absorbent foam in the silencer after a few shots and the silencer effectiveness is not satisfactory (Spence, 2009). To reduce the high frequencies which are due to the steep rise time of pressure signals from each individual air gun, a new air gun was designed and successfully tested (Coste *et al.*, 2014; Gerez *et al.*, 2015). Another mechanism is interaction between reflected ghost wave and air gun bubble which generates frequencies between 400 and 600 Hz (King *et al.*, 2015; King, 2015). A third high frequency generation mechanism is ghost cavitation (Landrø *et al.*, 2011). It was observed that a full air gun array, unlike single air guns or single arrays, has a much larger high frequency content compared to single guns. This signal occurs a few milliseconds after the ghost reflection (Landrø *et al.*, 2011). Such high frequencies are attributed to cavitation phenomena caused by reflected pressure signals from the water-air surface. These reflections are referred to as ghost signals, and hence the term ghost-cavitation is used for this phenomenon.

B. Acoustic waves and cavitation

Acoustic waves in a liquid can generate cavities. When the water pressure drops below the vapor pressure or partial pressure of the dissolved gases, there is a possibility of vapor or gas cavity formation in the liquid (Mellen, 1954; Plesset, 1970). The vapor cavity is called acoustic cavitation if it is from an oscillating pressure due to an acoustic wave propagating through a liquid (Frohly *et al.*, 2000; Apfel, 1984). The threshold pressure in an acoustic field that ruptures the water and creates cavitation varies significantly from moderate low pressures to high relative negative pressures. However, it is experimentally observed that the presence of cavitation nuclei facilitates cavity generation (Caupin and Herbert, 2006; Herbert *et al.*, 2006; Brennen, 2013). For example, in a venturi nozzle experiment, cavitation was observed when a small air bubble entered the low pressure region (Harrison, 1952). Cavitation collapse generates loud noise and high frequencies. For example, acoustic pressure is measured up to 0.7 MPa at a distance of 1–3 cm from cavity collapse from a snapping shrimp (Lohse *et al.*, 2001). The pressure inside a cavity at its minimum size is very high and might be up to thousands of bars (Mellen, 1954; Yasui *et al.*, 2010; Harrison, 1952). The cavitation noise is most severe when there are many collapsing cavities together, which is often denoted cloud cavitation (Reisman *et al.*, 1998). In the case of air gun arrays, ghost cavitation clouds can be formed because of the sudden pressure drop due to multiple reflected ghost signals from several single air guns in the array (Landrø *et al.*, 2011, 2013). This acoustically generated cavitation is assumed to be generated by a cavitation cloud and this hypothesis was further confirmed by more dedicated experiments (Landrø *et al.*, 2016).

C. Cavities in plasma due to an external electric field

It is interesting to note that there exists a surprisingly similar dynamical phenomenon in driven and damped plasmas. Plasmas are (partially) ionized gases, which imply that their dynamical properties are dominated by long range Coulomb forces acting between the charged particles (Pécseli, 2012). By driving plasma with an external electric field, an ensemble of cavities (density depressions or "cavitons") may form by means of a resonance mechanism (nucleation). Local high-frequency electric fields can be trapped in these cavities, inducing a collapse of the cavities until they become so small that they dissipate their energy as heat and sound waves (the burn-out) (Russell *et al.*, 1986; Hanssen *et al.*, 1992). Thereafter, the burnt-out cavities relax until they again become the nucleus for a new cycle of cavity nucleation, collapse, and burn-out. This phenomenon is called strong plasma turbulence (Russell *et al.*, 1986; Hanssen *et al.*, 1992), and it results in heating of the plasma, in addition to emission of sound and electromagnetic waves (Mjølhus *et al.*, 1995).

We believe that the similarity between nucleation-collapse-burnout dynamics in plasmas and cavitation-expansion-collapse in fluids is more than skin-deep. Hence, both systems

are governed by an external energy source (sound pulses in the case of seismic, electromagnetic waves in the case of plasma), and both kinds of cavities dissipate their energy to the surrounding medium as they dampen and finally collapse. The dynamics is inherently nonlinear, rendering the modeling and analysis difficult. The air gun generated bubble dynamics is in many ways the more complex of the two, as it involves phase transitions which do not take place in plasma turbulence. Also, under certain conditions hot and dense microplasma may be formed inside the vapor cavities, emitting electromagnetic waves (light and UV radiation) during their collapse (e.g., Bataller *et al.*, 2014; McNamara *et al.*, 1999). This connection between the plasma caviton collapse and vapor cavities collapse in fluids indicates interesting similarities between nonlinear fluid dynamics and nonlinear plasma dynamics. It is evident that the emitted sound and light from both types of collapse points to some deeper common underlying dynamics that is still poorly understood.

In this work we have modelled the ghost cavitation signal by assuming that the measured signal at any location is an aggregate of individual signatures from cavity collapses. To do so, temporal and spatial distribution regions around the air guns where cavities are more likely to be formed are required. The pressure values around the air guns are calculated based on air gun array signature modeling. Then, it is determined where and when the pressures drop below the assumed threshold level for cavitation growth. Afterwards, using bubble dynamics equations, the response of a microbubble, or impurities, to the estimated pressure from air gun arrays and their ghost is obtained. Having the cavitation signature corresponding to the estimated minimum pressure and its location and formation time, it is possible to forward propagate it to the receiver point. Geometrical spreading and absorption effects are included. Results of this modeling provide us with strong evidence that supports the ghost cavitation hypothesis. This work improves our understanding of one of the underlying mechanisms for the high frequency content of air gun arrays which might be used to develop strategies to reduce them. Even though we lack enough data regarding effects of noise on marine mammals we do not know how much these high frequencies bother or impact marine fauna. Hence, reducing the high frequency content is a correct strategy and a precaution. To our knowledge this is the first attempt to perform quantitative modeling of the ghost cavitation signal and compare the modeled results to far field measurements.

II. THE FIELD EXPERIMENT

The field experiment was conducted in 2008 in the Black Sea offshore Turkey. The source vessel was sailing along a straight line above a permanent hydrophone located at the sea bed. The shot interval was 25 m. The process is schematically shown in Fig. 1. The location of the hydrophone with respect to the closest shot is given by $x_0 = 1.2$ m, $y_0 = 39$ m, and $z_0 = 55$ m.

Normalized measured signals for shot number 15 to 25 and their 10 kHz high pass (HP) filtered signals are plotted together in Fig. 2. It is clear that shot 20 is the closest shot to the hydrophone.

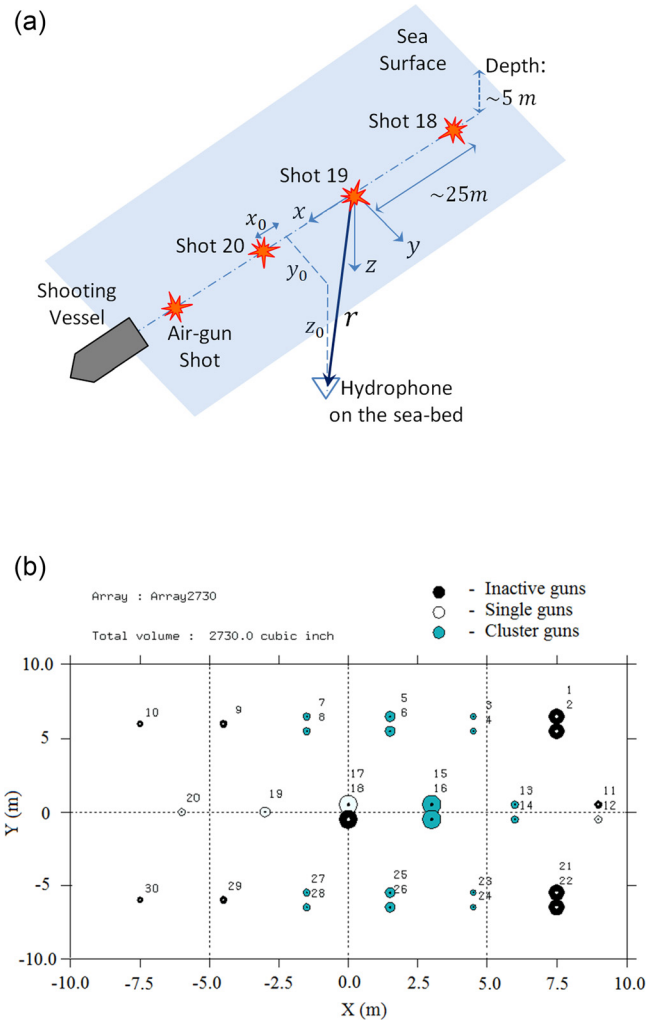

FIG. 1. (Color online) (Top) Schematic view of the field experiment; the hydrophone is stationary at the sea bed. The shooting vessel moves along a straight line above the hydrophone. The source depth is 5 m. (Bottom) The air gun array configuration seen from above.

We have plotted the normalized measured signal for shot 20—which is the nearest shot to the hydrophone—and its normalized 10 kHz HP filtered signal as well as the 200 Hz low pass (LP) filtered signal in Fig. 3. It is observed that the strong high frequency signal appears a few milliseconds after the surface ghost. The energy level of the high frequencies (>10 kHz) is around 50 to 60 dB less than the maximum energy level of the air gun signal which occurs between 50 to 100 Hz (Landrø *et al.*, 2011). To compare the relative magnitude of the low and high (>10 kHz) frequency signals the raw and the HP filtered signals are shown without normalization in Figs. 3(a) and 3(b), respectively. We observe that the amplitude of the high frequency signal is around 2%–3% of the amplitude of the raw signal. However, although the signal strength is weak compared to the low-frequency part of the air gun signature, these high frequencies might still influence marine mammal behavior. For example, the hearing of many of the odontocetes (toothed whales) is around 80 to 100 dB more sensitive in the frequency range from 10 to 100 kHz compared to lower frequencies (Ketten, 2004).

To have a reference point (zero time) for selecting the high frequency signals, the reference is chosen 5 ms after the

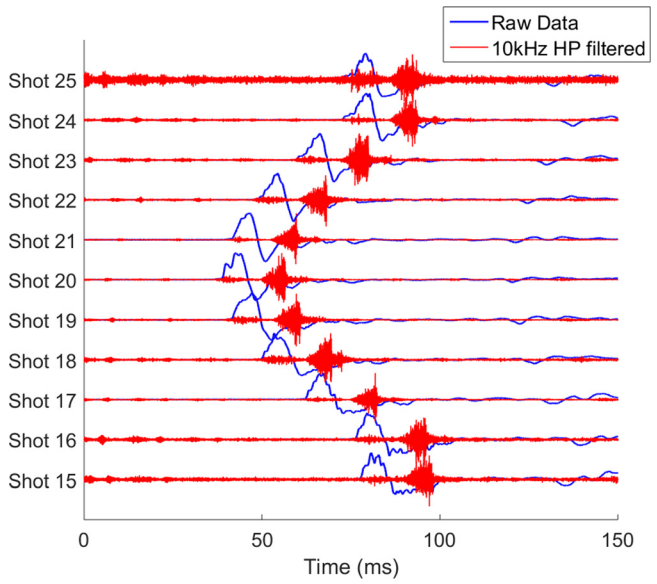

FIG. 2. (Color online) Normalized raw measured signals (blue lines) and their normalized 10 kHz HP filtered signal (red lines) for different shots 15 to 25.

peak time of the LP filtered signal for each shot. The reference point is important for comparing the measured field data with those from simulations which will be discussed later in this paper.

III. GHOST CAVITATION SIGNAL MODELING

When the content (which is water vapor molecules) of a cavity is highly compressed, the pressure inside the cavity is increased tremendously and its subsequent sudden collapse produces an intense acoustic signal (Brennen, 2005). There are several marine animals that create cavities in the water. The killer whale creates cavities by rapid movement of the tail. Another good example is the pistol shrimp which generates a cavity by snapping the claw (Versluis *et al.*, 2000). There are differences between collapses of a single cavity in the free field versus near boundaries and or presence of other cavities in its vicinity. A single cavity in free field collapses in a spherical shape without any liquid jet or vortex ring formation (Lauterborn and Hentschel, 1985). On the other hand, the cavities will be distorted due to the existing pressure field from other cavities or boundaries. Other effects related to cavity creation are jet formation, coalescence, or proliferation of cavities (Chew *et al.*, 2011). Furthermore, by solving the Keller-Miksis equation numerically (Li *et al.*, 2013), it was shown that the presence of a smaller cavity intensifies the pressure pulse of bigger ones compared to isolated cavities and is maximized when the cavities have equal initial radii. Experimental results also show that severe cavitation noise and very large pressure pulses occur when many cavities collapse within a cloud in close proximity to each other (Reisman *et al.*, 1998; Wang and Brennen, 1995). Despite the fact that interaction between cavities is complex, Harrison (1952) argues that the noise spectrum from a cloud of cavities can be considered to be formed by summation of pulses from individual cavities. Hence, we will assume a simple model for our modeling, assuming a simple superposition of individual cavities that collapse.

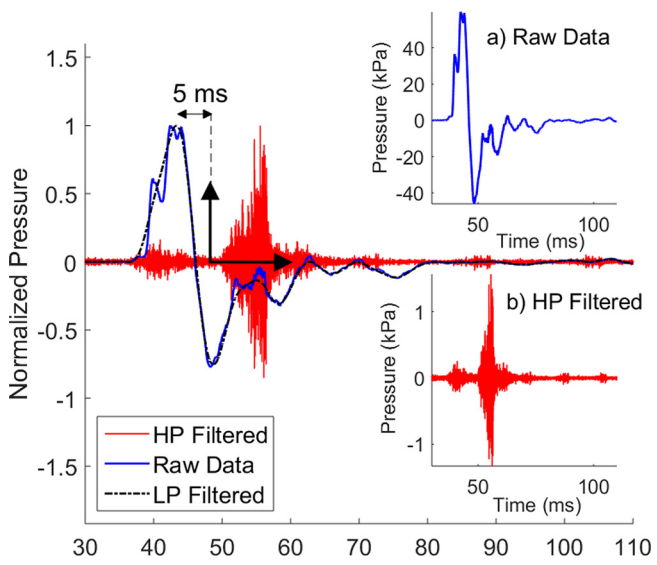

FIG. 3. (Color online) Normalized raw measured signal (blue line) for shot 20 and its normalized 10 kHz HP filtered signal (red line). The corresponding LP filtered signal is shown as a black dashed-dotted line. The reference point (zero time) for the HP filtered signal is shown by thick black axes. To compare the magnitude of high frequencies with the measured signal, raw measured signal at hydrophone and its 10 kHz high passed filtered signal are also plotted without normalization in (a) and (b), respectively.

A. Modeling the pressure drop caused by reflected air gun signals from the sea surface

Reflected acoustic pressure waves from the sea surface have opposite polarity compared to the positive incident wave from individual air guns in an air gun array. This reversal is due to the fact that the reflection coefficient of pressure waves is close to −1 for the water-air interface. It is important to stress that this polarity reversal occurs for the relative or dynamic pressure, which is the acoustic pressure relative to the hydrostatic pressure. This means that the absolute pressure in the water is never negative, however, when the dynamic pressure is negative, the absolute pressure will approach zero, and cavity creation will then occur. Such negative pressure created by the ghost signals from many individual air guns might "add up" in some regions and cause the absolute hydrostatic pressure to approach zero. To find the spatial and temporal distribution of the absolute hydrostatic pressure in the water and map when and where it approaches zero, we use air gun modeling (Ziolkowski, 1970). We model the acoustic pressure generated by the air gun array in a volume surrounding the array. This volume is divided into small cells using a grid resolution of 0.2 m and a computational time sampling of 0.1 ms. Using these dense values for time and space discretization ensures no spatial and temporal aliasing in the modeling of the pressure.

The regions where the absolute hydrostatic pressure of water is less than −0.1 bar are shown at four different time instants in the top row of Fig. 4. Here it should be noted that the air gun modeling theory is based on linear superposition

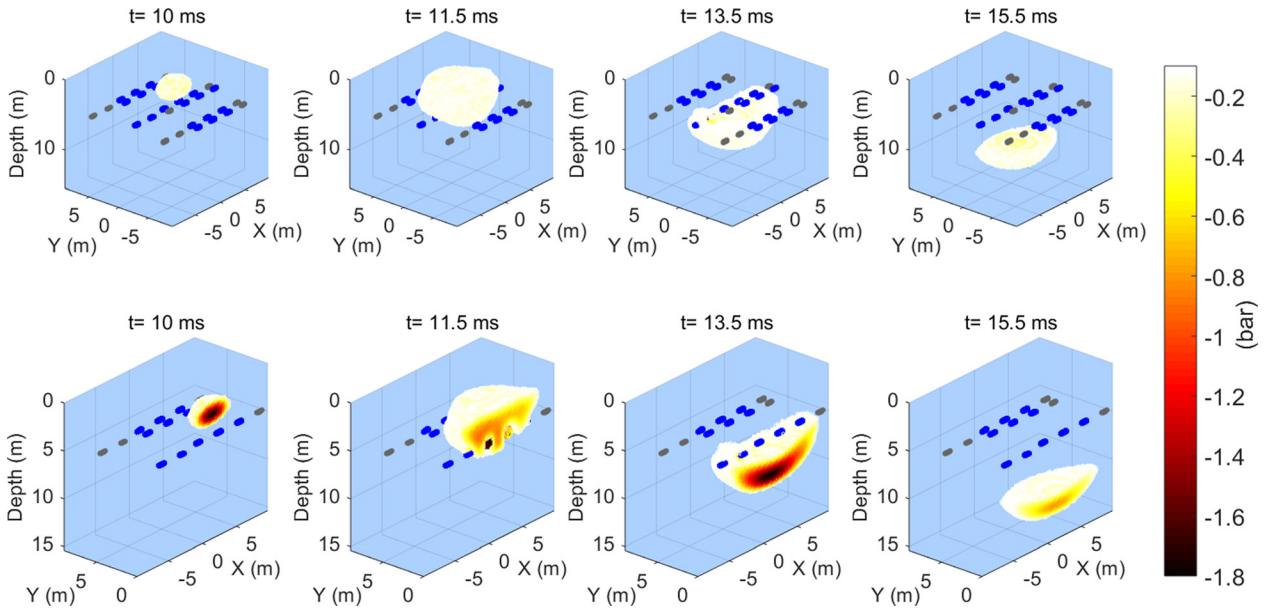

FIG. 4. (Color online) Top row: regions where the absolute hydrostatic pressure is less than −0.1 bar at four time instants. The computational domain is divided to the cells of 0.2 m and time resolution is 0.1 ms. The active air guns in the arrays are shown in blue while the inactive air guns are shown in gray. Bottom row: cut sections of images shown in the top row (to visualize where the minimal pressures occur).

when the pressure contribution from each air gun is added, and the actual number of −0.1 bar is an assumption which is found practical to achieve a reasonable match between modeled and measured data. As the absolute pressure in the water approaches zero, the superposition principle breaks down due to non-linear effects which are not accounted for in the modeling software we use. Since each air gun is considered as a point source in the computational domain and the released pressure from each air gun will be scaled by the inverse of the propagation distance (geometrical spreading), for the near points to the source the pressure becomes unrealistically high. Therefore we exclude grid cells closer than 0.5 m from each air gun when calculating the pressure field from that air gun. The active and inactive air guns in the arrays are shown by blue and gray colors, respectively, in Fig. 4.

In the second row of Fig. 4, cut sections of the figures from the top row are plotted. In the cut sections the pressure distributions inside the cavity cloud are better observed.

B. Cavity collapse

There are several approaches to model the acoustic pressure generated by cavity collapses. One way is to only consider the collapse of the cavities after they reach their maximum size and neglecting the underlying mechanism from initiation to maximum size growth. The other way, which is our approach in this paper, is to consider cavity generation, growth, and subsequent collapse. We assume there are small particles, impurities, or tiny bubbles in the sea water as potential nucleation sites. These nucleation sites just help the formation of cavities in the way that cavities attach to these impurities and grow. If there are multiple heterogeneities in the water—multiple cavities will form—leading to a randomized collapse of several thousand cavities. A microbubble can exist in stable equilibrium if its radius is smaller than the Balke critical radius (Brennen, 2013). Such nucleation sites exist in the seawater with typical radii between 1 and 100 μm (Ceccio and Brennen, 1991; Brennen, 2013). In addition, the collapsing cavities themselves act as nuclei sites for continued generation of cavities and therefore the cavitation rate increases (Ceccio, 1990). As the external pressure around the nucleation site decreases, the cavity starts growing rapidly and subsequently the pressure inside the cavity decreases and molecules of water will be transferred to the cavity as water vapor. Due to rapid growth of the cavity, the pressure inside it falls below the pressure outside the cavity and therefore the cavity shrinks violently and collapses.

We assume that the tiny stable bubble with radius R_0 is filled with air—or water vapor—and the initial pressure, P_0, inside the stable free bubble (no bubble wall motion) is estimated from the following equation (Woolf, 2001):

$$P_0 = P_{\text{atm}} + \rho g z + \frac{2\sigma}{R_0}. \tag{1}$$

In the above equation, $\sigma = 0.074$ N/m is water surface tension (Nayar *et al.*, 2014), ρ is the density of water, z is the depth where free microbubbles exist, g is acceleration of gravity, and P_{atm} is the atmospheric pressure.

The response of such a tiny free stable bubble—which acts as a cavity nucleation site—subjected to external pressure, P, can be estimated from the following bubble dynamics equation (Prosperetti and Lezzi, 1986):

$$\begin{aligned}\left(1-\frac{1}{c}\frac{dR}{dt}\right)R\frac{d^2R}{dt^2}+\frac{4\mu}{\rho c}\frac{d^2R}{dt^2}&\\ =-\frac{3}{2}\left(1-\frac{1}{3c}\frac{dR}{dt}\right)\left(\frac{dR}{dt}\right)^2-\frac{1}{\rho R}\left[2\sigma+4\mu\frac{dR}{dt}\right]&\\ +\frac{1}{\rho}\left(1+\frac{1}{c}\frac{dR}{dt}\right)[P_i(t)-P]+\frac{R}{\rho c}\frac{dP_i(t)}{dt}.&\end{aligned} \tag{2}$$

Here, $R(t)$ is the time dependent radius of the cavity, c is sound speed of undisturbed water, and μ is the dynamic viscosity of water. The pressure inside the cavity, $P_i(t)$, is modelled by the Van der Waals equation

$$P_i(t) = P_0 R_0^{3k} (R(t))^{-3k}. \tag{3}$$

In the above equation, $k = 1$ for isothermal processes, and for adiabatic processes $k = 1.4$.

The magnitude of the actively emitted pressure component from a body with volume oscillations (e.g., breathing sphere or bubble) at far-field, located at distance r from the sphere center, can be estimated by the following equation (Hilgenfeldt *et al.*, 1998; Brennen, 2013; Leighton, 2012) if the dimension of volume is much smaller than the emitted sound wavelength:

$$p(t) = \frac{\rho}{4\pi r}\frac{d^2V}{dt^2} = \frac{\rho R(t)}{r}\left(2\dot{R}^2(t) + R(t)\ddot{R}(t)\right). \tag{4}$$

The response of a stable microbubble with initial radius $R_0 = 20\,\mu$m at two different locations in the computational domain around the air gun array are subjected to the pressure changes due to the air gun array as depicted by the blue dashed lines in Fig. 5 (top row). The cavitation radius variations are estimated solving Eq. (2) by means of the Runge-Kutta method of order 5 ("ode45" algorithm in MATLAB) and are shown by red solid lines in the top row. Pressure responses from cavitation collapse at $r = 1$ m from the cavity center are estimated by Eq. (4) and plotted in the second row in Fig. 5.

The responses of several different cavities at different locations (depths) of the computational domain subjected to the external pressures at those locations are estimated by solving the bubble dynamic Eq. (2). The maximum cavity growth, collapse time, and peak pressure from modeled cavity collapses are extracted from the simulations and plotted as a function of minimum external pressures and depth in Figs. 6(a)–6(c), respectively. Two trends are observed: first, decreasing the external minimum pressures increases the collapse time and the cavity growth is larger. Second, for the same minimum external pressure, deeper cavities have shorter collapse times and smaller cavity radii. The collapse time increase by the decrease of the hydrostatic pressure is quantitatively in agreement with Rayleigh's (1917) equation

$$T = 0.915 R_{\max}\sqrt{\rho/P_h}, \tag{5}$$

where T is the collapse time of the cavity, $R_{\max}$ is its maximum radius, and P_h is the hydrostatic pressure surrounding the cavity.

It should be noted that the magnitude of minimum external pressure and the water depth are not the only factors that affect the cavity growth and collapse. Another factor is the width of the minimum external pressure. The total pressures produced by the air gun array are plotted for few points shallower than 8 m in Fig. 6(d) and for some deeper points in Fig. 6(e). We observe that for shallow points (<8 m) the shapes of the pressure curves are not similar and their minimum pressure widths are different. However the pressures at deeper points (>8 m) have similar shapes and practically the same width for their "minimum" main valleys. That is why the linear relation that is observed between 8 and 15 m depth does not persist to the shallower depths [see Figs. 6(a)–6(c)].

For four different locations shown as colored dots in the above figures, their corresponding cavity signatures are plotted in Fig. 7. To be able to compare different cavity growth and collapse signatures, the external pressures [P in Eq. (2)] are shifted in a manner to have their minimum pressures at 10 ms. It is observed that the cavity starts growing around 0.4 ms before the external pressure reaches its minimum

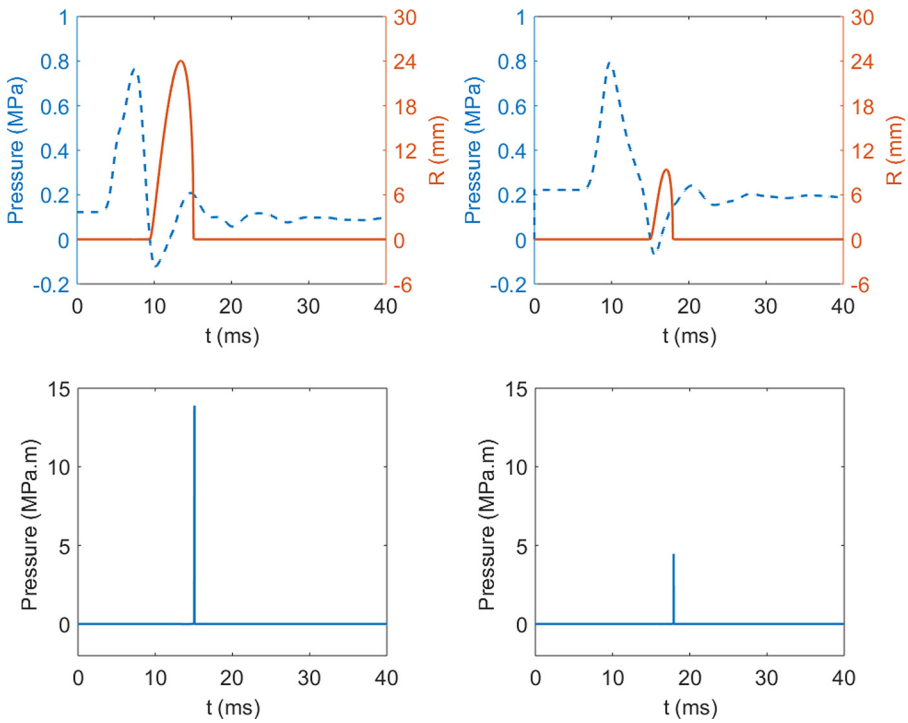

FIG. 5. (Color online) Response of a free stable bubble with initial radius ($R_0 = 20\,\mu$m) located at ($x = 1.2$ m, $y = -0.1$ m, $z = 2.2$ m) subject to simulated external pressure from air-gun arrays at that point (left) and the response of same bubble located at ($x = 1.6$ m, $y = 0.3$ m, $z = 12.4$ m) subject to simulated external pressure from air-gun arrays at that point (right). The external pressures are plotted with a blue dashed line. The second row shows the pressure signature at 1 m from the cavity collapse in the first row.

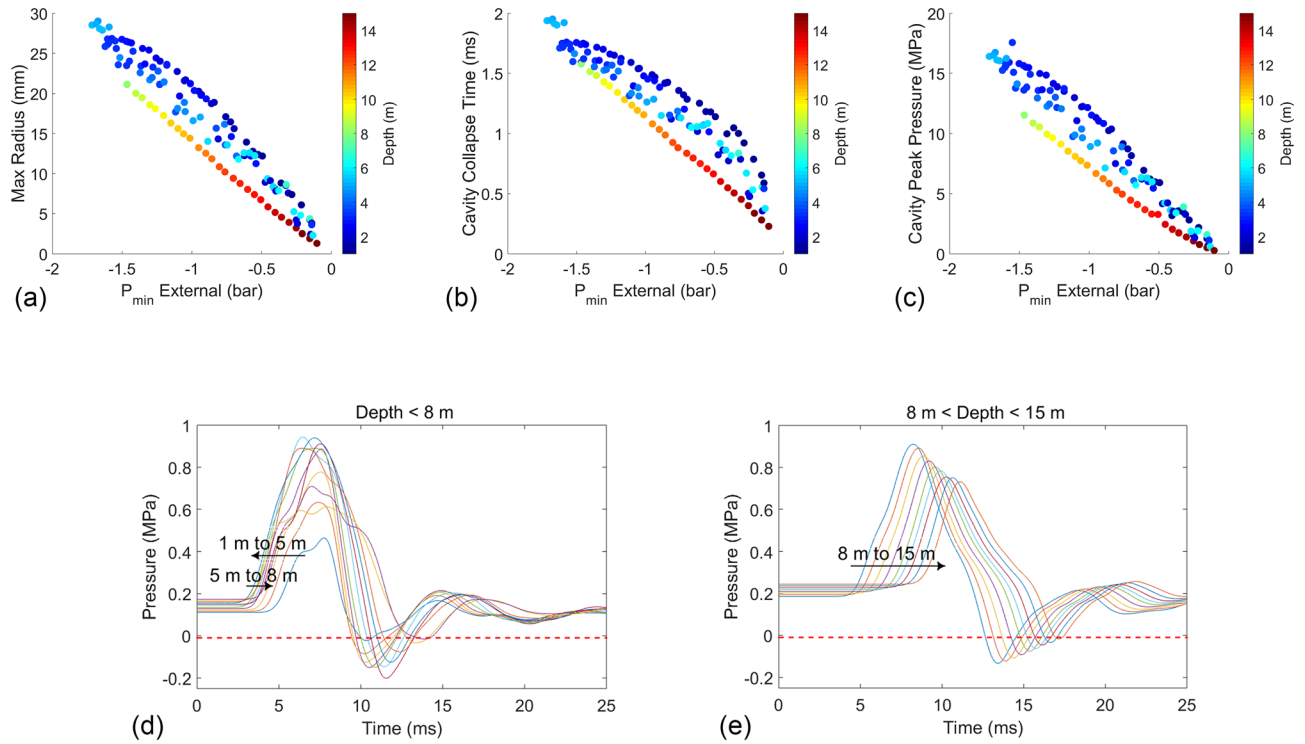

FIG. 6. (Color online) Response of a free stable bubble with initial size of 20 μm at different points in the computational domain around the air-gun array subjected to external pressures from the air-gun array (and hydrostatic pressure) at that point using Eq. (2). (a) Maximum cavity radius growth vs minimum external pressures at different points. (b) Cavity collapse time vs minimum external pressures at different points. (c) Cavity peak pressure vs minimum external pressures at different points. (d) Total external pressure at some points located shallower than 8 m. (e) Total external pressure at some points located deeper than 8 m. In (d) and (e) the red dashed line shows the -0.1 bar (-0.01 MPa) threshold pressure.

value. Furthermore, it is seen that for almost the same minimum pressure, the collapse time is shorter for deeper points corresponding to higher hydrostatic pressures.

In Fig. 4 it is shown when and where the hydrostatic pressure drops below the assumed threshold pressure (-0.1 bar). By solving Eq. (2) and from Fig. 5 it is observed that having the time when the external pressure reaches its' minimum at each point it is required to know when the cavity starts growing and its subsequent collapse at each point within the computational domain. Spatial and temporal distributions of minimum pressures are plotted at four different time instants in Fig. 8.

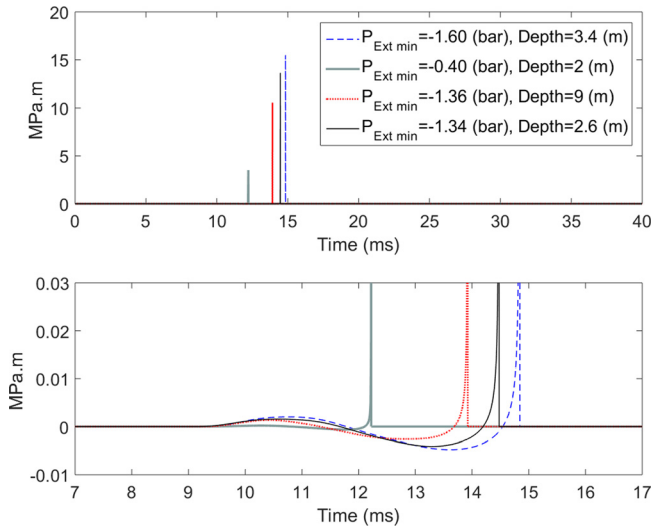

FIG. 7. (Color online) Cavity signatures at four different points in the computational domain.

C. Propagation of cavity signatures from source to receiver

In Secs. III A and III B, the temporal and spatial distribution of pressures less than -0.1 bar (the threshold pressure) and also the pressure signature from cavitation collapses at different depth and for different minimum pressures were calculated. In addition to the shape of individual cavity signatures, relative arrival time of individual signatures affects the measured signal at the receiver. The arrival time of the signal from each cavity depends on the formation time of the cavity denoted by τ, time of collapse T, and the travel time (or distances) from cavity to receiver. The term $1/r$ represents geometrical spreading. In other words, spatial and temporal distributions of cavities affect the shape of the measured signal at the receiver. Absorption effects are included in our model since the signal generated by the cavity has a high frequency content.

Absorption, γ (Neper/m), is calculated from the equation given by Francois and Garrison (1982). In the model three different dissipation mechanisms are considered: (i) viscosity of pure water which is effective at high frequencies, (ii) relaxation of magnesium sulfate molecules which is dominant at frequencies below 100 kHz, and (iii) relaxation of boric acid molecules which is significant at frequencies below 1 kHz. The effect of the ith cavity bubble recorded by

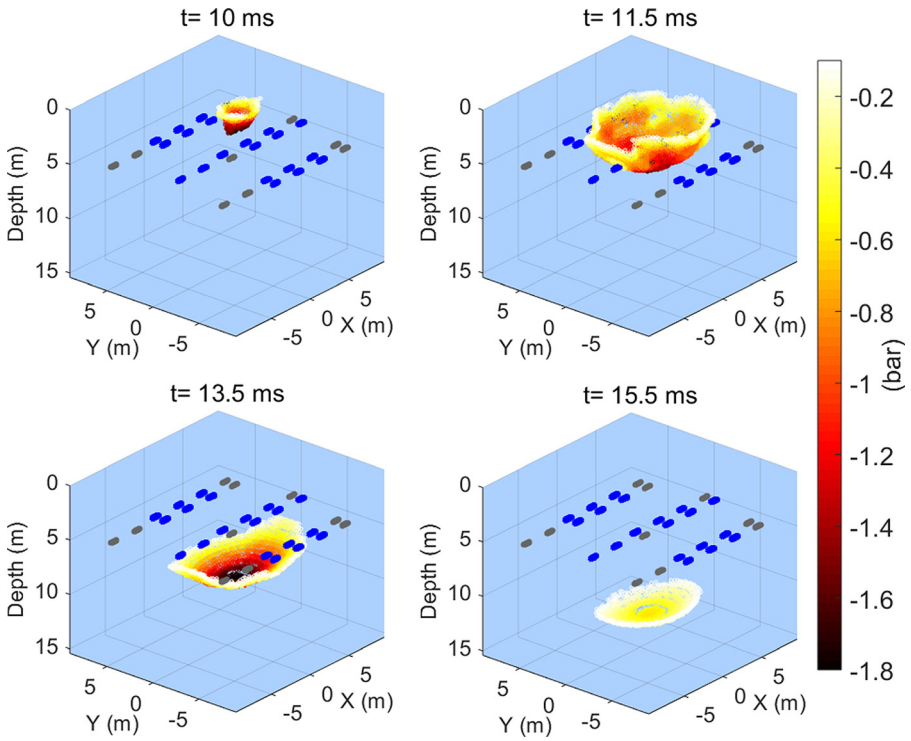

FIG. 8. (Color online) The locations in the computational domain which reach their minimum pressure at four instants of time ($t = 10$, 11.5, 13.5, 15.5 ms). The plotting threshold was chosen to -0.1 bar.

the hydrophone is given by u_i and is obtained by the following formula:

$$u_i(t,r) = \frac{1}{\sqrt{2\pi}} \int_{-\infty}^{+\infty} \left(S_i(f) \cdot e^{-\gamma(f) r_i} \cdot e^{-j2\pi f \tau_i} \cdot \frac{e^{-j(2\pi f/c) r_i}}{r_i} \right) \times e^{j2\pi t f} df. \tag{6}$$

Here $S_i(f)$ is the frequency domain representation of the time signal from the collapse of the ith cavity and $j = \sqrt{-1}$ is the imaginary unit. The distance of the cavity from the hydrophone is r_i and its formation time is τ_i. We have used MATLAB to calculate the inverse Fourier transform in Eq. (6). After having the effect of each cavity, the total effect is obtained by linear superposition, as suggested by Harrison (1952), and denoted by $y(t)$:

$$y(t,r) = \sum_{i=1}^{N} u_i. \tag{7}$$

In Eq. (7), N is the number of grid points for which pressure reaches its minimum and is smaller than the assumed threshold for cavity initiation.

IV. RESULTS

Ghost cavity cloud signals are simulated by considering the aggregate effects of the collapse of individual cavities in the receiver location. The method is summarized by the following steps:

Step 1. Cavities growth initiation times are required. Therefore we need to know at each grid point in the computational domain, at what time the pressure reaches its minimum and whether its magnitude is below assumed threshold pressure (-0.1 bar) for cavity generation. This information is depicted in Fig. 8 at four time instants. We have such information for every 0.1 ms from the simulation.

Step 2. The cavity signature at each point is selected based on the magnitude of negative pressure obtained in (step 1) and its depth from a cavity signature library (Figs. 6 and 7).

Step 3. Such cavities are propagated from where they are formed to the receiver point. Absorption and geometrical spreading is included in propagation from source to receiver as explained in Sec. III C.

In the following we have assumed two cases: (1) no interaction between cavities, this is called model 1, and (2) pressure interaction between the cavity collapses which is called model 2. From an implementation point of view, the difference between the two models is in step 2. In model 1, cavities are selected directly based on the magnitude of minimum pressure in step 1. In the second case, cavity signatures are selected based on a weighted magnitude of minimum pressures given in step 1. The weighting is based on the simple model that as the time passes the pressure from collapses of cavities elevate the minimum pressure given in step 1.

A. Model 1—No interaction between cavities

In this case it is assumed that there is no effect from the former cavity collapses on the later ones. Thus, the cavity signature at each point is selected directly based on the minimum pressure at that point and the depth information without further manipulation. The 10 kHz HP filtered simulated ghost cavitation signal for shot 20 together with the far-field signature from air guns array and its LP filtered signal are plotted in Fig. 9.

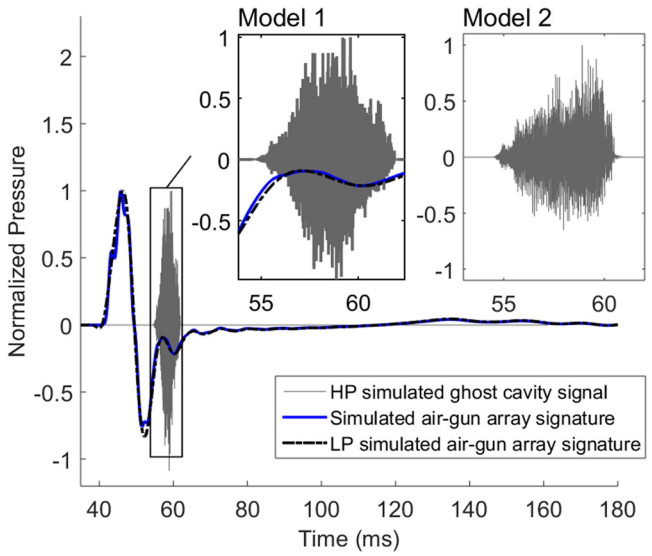

FIG. 9. (Color online) Simulated air-gun far-field signature and its LP filtered signature together with the 10 kHz HP filtered simulated ghost cavity signal for shot 20 using model 1. Simulated 10 kHz HP filtered signal for shot 20 by assuming pressure interaction between cavities is also plotted (model 2). All signals are normalized.

B. Model 2—With pressure interaction between cavities

The cavity interaction is included based on the assumption that collapses of initial cavities produce intense pressures which increase the hydrostatic pressure around cavities that are formed later. Therefore, the collapse time and growth of the cavities that are formed at later times are reduced. This can be justified by modifying the Rayleigh cavity collapse time equation

$$T = 0.915R\sqrt{\rho \Big/ \left(P_h + \sum_i^N P_i\right)}. \tag{8}$$

The summation of pressures in the denominator of Eq. (8) models the effects of cavity collapses which is analogous to the pressure field interactions in an air gun array [see Eq. (8) in Ziolkowski *et al.* (1982)]. Therefore, in this part it is assumed that cavities that are generated at earlier times are formed only due to the external pressure from air gun array and are not affected by other cavity collapses. While the cavities that are formed at later times are more and more affected by previous cavities and consequently they grow less, have shorter collapse times, and less intense peaks.

In this model, at the beginning (during the first 0.5 ms) of ghost cloud formation cavities are selected solely based on the estimated pressure drops from air gun array and as the time passes the collapse time of cavities (and their growth) that are formed later are deceased gradually. Then it is assumed gradual collapse time decreases by 50% and then 80% at the end of the process compared to the case without any pressure interaction between cavities. These values for the model are obtained after few trial and errors. The results for 10 kHz HP-filtered simulated signal for shot 20 is shown in Fig. 9.

Using the 5 ms after peak time of LP filtered array signature as a reference for the ghost cavitation signal (the same reference as in field measured data), normalized cumulative energies of a 10 kHz HP filtered signal from field measurement and simulation from models 1 and 2 for shot 20 are plotted in Fig. 10 (top) and the absolute value of difference between two models is plotted underneath the same figure. It is observed that there is a good match between simulation results and field measurement. However, for model 1, the shape of the HP filtered simulated ghost cavitation signal (Fig. 9) does not resemble the shape of the measured field data. Compared to model 1, it is observed that model 2 has a better agreement with the field data. The normalized cumulative energy from model 2 fits well with the field data from around 15% to 90% energy accumulation curve of the field data. In addition, the envelope of the simulated signal from model 2 has skewness which better agrees with the skewness of HP filtered signal's envelopes from field experiment.

Figure 11 shows a comparison between normalized HP filtered simulated signals (left) and measured signals (right) for shots 15 to 20.

There is an interesting skewness of the envelope of both the modeled and measured signatures in Fig. 11, as pointed out by Landrø *et al.* (2016). There are several factors that must be taken into account to explain this skewness. Those factors include dimensions of the cloud, size, and number of cavities, the downward speed of the cavitation cloud (see Fig. 4), and the relative location of the receiver to the cavitation cloud. Both size and number of cavities are maximum at the shallower depths (<5 m) and as the cavitation cloud moves downwards, the distance between cavities and receiver decreases and therefore weaker signals that are formed later are received by the hydrophone a little earlier than the cavities generated at shallower depths. In addition, the collapse time of each cavity increases linearly with radius [Eq. (5)]. Hence we see that the signal "swells" to its maximum and then vanishes much more quickly.

The duration of the ghost cavitation signal increases as the incident angle (measured relative to the vertical line)

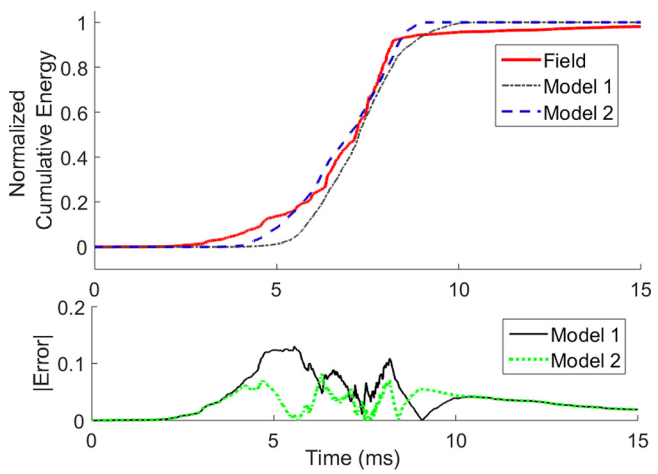

FIG. 10. (Color online) Top panel: Normalized cumulative energies of 10 kHz HP filtered simulated signal from models 1 and 2. Bottom panel: The absolute value of the difference between normalized cumulative energy curves of field data and the two models.

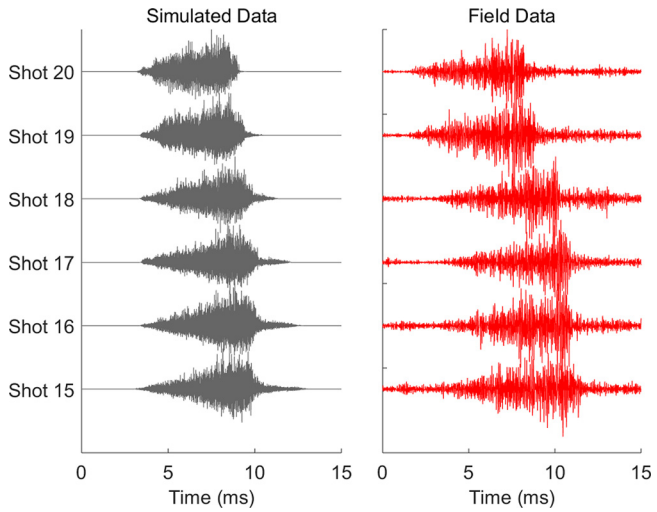

FIG. 11. (Color online) Simulated (left) and field experiment (right) 10 kHz HP-filtered signal for different shot numbers 15 to 20 from model 2. The shot receiver configuration is shown in Fig. 1 (left). The signals are selected 5 ms after the first main peak of the LP filtered array signature.

increases. This effect is mainly caused by the finite extension of the cavity cloud. The width of the signal increases from approximately 6 ms for shot 20 to 7.5 ms for shot 15.

V. DISCUSSION AND CONCLUSIONS

We have developed a modeling scheme that incorporates the creation of water vapor cavities due to acoustic stimulation by multiple ghost reflections from air guns that are fired simultaneously when marine seismic data are acquired. The first modeling step is to model the low-frequency signal of an air gun array. The theory for this is well known, and we use this first modeling step to determine the spatial and temporal distribution of regions where cavities are likely to occur. When the acoustic signals from several air guns are reflected from the sea surface, simple superposition is used to calculate the pressure at a given water depth. Using this linear superposition principle predicts some regions to have negative absolute pressure values. This means that the linear theory breaks down, and as a simple solution, we assume that cavities are formed when the linear acoustic theory breaks down. By assuming that cavities are formed at locations where this happens, we model multiple cavities. In the current version we assign one cavity to each grid point in the computational domain. In the present examples we have used a grid size of 0.2 m. This is an assumption, and the number of cavities can be increased by decreasing the grid size.

The cavity growth and collapse are modeled using the Keller bubble dynamic equations. It is assumed that a cavity starts growing when the pressure around it reaches the minimum value (we used −0.1 bar in our examples). The basic assumption is that there are infinitesimal impurities in the water, which act as nuclei for cavity growth. When the output acoustic signal from one single cavity is modeled, geometrical spreading is included by multiplication of the inverse source-receiver distance. Absorption effects are included by using a simple Q-model, where Q-values are calculated by the equation given by Francois and Garrison (1982).

We find that the maximum cavity radius increases close to linearly with the modeled minimum pressure. In addition to this trend, there is a weaker trend related to the depth of the cavity: shallow cavities have a slightly larger maximum radius than the deeper cavities. The cavity collapse time follows Rayleigh's equation.

In our modeling we have not included the effect of transmission losses and ray bending due to the presence of a cavity cloud. Especially if the cloud is dense, such effects might alter our modeling results significantly, both with respect to travel-time and amplitudes. In addition, more sophisticated cavity interaction models will be investigated further in the future.

The results indicate a good correspondence between modeled and measured high frequency signals. By correspondence we mean a similar envelope of the chaotic high frequency signal, not details corresponding to the collapse of single cavities. Accounting for interaction between cavities by assuming that the radiated pressure from all other cavities are changing the hydrostatic pressure surrounding one cavity improves this correspondence. The onset time and the duration of the high-frequency cavitation signal fits reasonably well between modeled and measured data. The modeled average maximum cavity radius is 9.8 mm for the initial model and it is 3.9 mm for the model with cavity interaction.

In this work we have compared modeled and measured high frequency signals after normalizing. A calibration step could involve a scaling of the modeled signature from individual cavity collapses and/or adjusting the number of cavities. In the current modeling example we used a relatively high number of cavities, assuming that each grid point fulfilling the minimum pressure threshold hosts a cavity. However, there is obviously a tradeoff between the strength of each cavitation signal and the number of cavities.

We suggest that our model can be used to design seismic air gun arrays which produce less high-frequency signals.

ACKNOWLEDGMENT

This research is funded by Research Center for Arctic Petroleum Exploration (ARCEx) partners, and the Research Council of Norway (Grant No. 228107). The reviewers are acknowledged for their constructive comments and invaluable suggestions.

Apfel, R. E. (**1984**). "Acoustic cavitation inception," Ultrasonics **22**(4), 167–173.
Askeland, B., Hobæk, H., and Mjelde, R. (**2007**). "Marine seismics with a pulsed combustion source and Pseudo Noise codes," Marine Geophys. Res. **28**(2), 109–117.
Barger, J. E., and Hamblen, W. R. (**1980**). "The air gun impulsive underwater transducer," J. Acoust. Soc. Am. **68**(4), 1038–1045.
Bataller, A., Kappus, B., Camara, C., and Putterman, S. (**2014**). "Collision time measurements in a sonoluminescing microplasma with a large plasma parameter," Phys. Rev. Lett. **113**(2), 024301.
Bouyoucos, J. V. (**1975**). "Hydroacoustic transduction," J. Acoust. Soc. Am. **57**(6), 1341–1351.
Brennen, C. E. (**2005**). *Fundamentals of Multiphase Flow* (Cambridge University Press, London), Chap. 5.

Brennen, C. E. (**2013**). *Cavitation and Bubble Dynamics* (Cambridge University Press, London).
Caldwell, J., and Dragoset, W. (**2000**). "A brief overview of seismic air-gun arrays," Leading Edge **19**(8), 898–902.
Caupin, F., and Herbert, E. (**2006**). "Cavitation in water: A review," Comptes Rendus Physique **7**(9), 1000–1017.
Ceccio, S. L. (**1990**). "Observations of the dynamics and acoustics of travelling bubble cavitation," Ph.D. thesis, California Institute of Technology Pasadena, California.
Ceccio, S. L., and Brennen, C. E. (**1991**). "Observations of the dynamics and acoustics of travelling bubble cavitation," J. Fluid Mech. **233**, 633–660.
Chelminski, S. (**2015**). "Device for marine seismic explorations for deposits," U.S. patent 8,971,152 B2 (February 23, 2014.)
Chew, L. W., Klaseboer, E., Ohl, S. W., and Khoo, B. C. (**2011**). "Interaction of two differently sized oscillating bubbles in a free field," Phys. Rev. E **84**(6), 066307.
Coste, E., Gerez, D., Groenaas, H., Hopperstad, J. F., Larsen, O. P., Laws, R., Norton, J., Padula, M., and Wolfstirn, M. (**2014**). "Attenuated high-frequency emission from a new design of air-gun," in *84th Annual International Meeting*, SEG, Expanded Abstracts, pp. 132–137.
Dragoset, B. (**2000**). "Introduction to air guns and air-gun arrays," Leading Edge **19**(8), 892–897.
Duren, R. E. (**1988**). "A theory for marine source array," Geophysics **53**(5), 650–658.
Erbe, C., and Farmer, D. M. (**2000**). "A software model to estimate zones of impact on marine mammals around anthropogenic noise," J. Acoust. Soc. Am. **108**(3), 1327–1331.
Francois, R. E., and Garrison, G. R. (**1982**). "Sound absorption based on ocean measurements. Part II: Boric acid contribution and equation for total absorption," J. Acoust. Soc. Am. **72**(6), 1879–1890.
Frohly, J., Labouret, S., Bruneel, C., Looten-Baquet, I., and Torguet, R. (**2000**). "Ultrasonic cavitation monitoring by acoustic noise power measurement," J. Acoust. Soc. Am. **108**(5), 2012–2020.
Gerez, D., Groenaas, H., Larsen, O. P., Wolfstirn, M., and Padula, M. (**2015**). "Controlling air-gun output to optimize seismic content while reducing unnecessary high-frequency emissions," in *2015 Society of Exploration Geophysicists Annual Meeting*.
Goold, J. C., and Fish, P. J. (**1998**). "Broadband spectra of seismic survey air-gun emissions, with reference to dolphin auditory thresholds," J. Acoust. Soc. Am. **103**(4), 2177–2184.
Gordon, J., Gillespie, D., Potter, J., Frantzis, A., Simmonds, M. P., Swift, R., and Thompson, D. (**2003**). "A review of the effects of seismic surveys on marine mammals," Mar. Technol. Soc. J. **37**(4), 16–34.
Hanssen, A., Mjolhus, E., DuBois, D. F., and Rose, H. A. (**1992**). "Numerical test of the weak turbulence approximation to ionospheric Langmuir turbulence," J. Geophys. Res. **97**(A8), doi:10.1029/92JA00874 12073–12091.
Harrison, M. (**1952**). "An experimental study of single bubble cavitation noise," J. Acoust. Soc. Am. **24**(6), 776–782.
Herbert, E., Balibar, S., and Caupin, F. (**2006**). "Cavitation pressure in water," Phys. Rev. E **74**(4), 041603.
Hildebrand, J. A. (**2009**). "Anthropogenic and natural sources of ambient noise in the ocean," Mar. Ecol. Progr. Ser. **395**, 5–20.
Hilgenfeldt, S., Lohse, D., and Zomack, M. (**1998**). "Response of bubbles to diagnostic ultrasound: A unifying theoretical approach," Eur. Phys. J. B **4**(2), 247–255.
Ketten, D. R. (**2004**). "Marine mammal auditory systems: A summary of audiometric and anatomical data and implications for underwater acoustic impacts," Polarforschung **72**(2–3), 79–92.
King, J. R. (**2015**). "Air-gun bubble-ghost interactions," Geophysics **80**(6), T223–T234.
King, J. R. C., Ziolkowski, A. M., and Ruffert, M. (**2015**). "Boundary conditions for simulations of oscillating bubbles using the non-linear acoustic approximation," J. Comput. Phys. **284**, 273–290.
Landrø, M., and Amundsen, L. (**2010**). "Marine seismic sources. Part I," Geo ExPro **7**(1), 32–34.
Landrø, M., Amundsen, L., and Barker, D. (**2011**). "High-frequency signals from air-gun arrays," Geophysics **76**(4), Q19–Q27.
Landrø, M., Amundsen, L., and Langhammer, J. (**2013**). "Repeatability issues of high-frequency signals emitted by air-gun arrays," Geophysics **78**(6), P19–P27.
Landrø, M., Ni, Y., and Amundsen, L. (**2016**). "Reducing high-frequency ghost cavitation signals from marine air-gun arrays," Geophysics **81**(3), P33–P46.
Lauterborn, W., and Hentschel, W. (**1985**). "Cavitation bubble dynamics studied by high speed photography and holography: Part one," Ultrasonics **23**(6), 260–268.
Leighton, T. (**2012**). *The Acoustic Bubble* (Academic Press, New York).
Li, F., Cai, J., Huai, X., and Liu, B. (**2013**). "Interaction mechanism of double bubbles in hydrodynamic cavitation," J. Therm. Sci. **22**(3), 242–249.
Lohse, D., Schmitz, B., and Versluis, M. (**2001**). "Snapping shrimp make flashing bubbles," Nature **413**(6855), 477–478.
Madsen, P. T., Johnson, M., Miller, P. J. O., Soto, N. A., Lynch, J., and Tyack, P. L. (**2006**). "Quantitative measures of air-gun pulses recorded on sperm whales (Physeter macrocephalus) using acoustic tags during controlled exposure experiments," J. Acoust. Soc. Am. **120**(4), 2366–2379.
McCauley, R. D., Fewtrell, J., Duncan, A. J., Jenner, C., Jenner, M. N., Penrose, J. D., Prince, R. I., Adhitya, A., Murdoch, J., and McCabe, K. (**2000**). "Marine seismic surveys: Analysis and propagation of air gun signals and effects of air gun exposure on humpback whales, sea turtles, fishes and squid," Curtin University of Technology, Project CMST, Perth, Australia, Vol. 163.
McNamara, W. B., Didenko, Y. T., and Suslick, K. S. (**1999**). "Sonoluminescence temperatures during multi-bubble cavitation," Nature **401**(6755), 772–775.
Mellen, R. H. (**1954**). "Ultrasonic spectrum of cavitation noise in water," J. Acoust. Soc. Am. **26**(3), 356–360.
Mjølhus, E., Hanssen, A., and DuBois, D. F. (**1995**). "Radiation from electromagnetically driven Langmuir turbulence," J. Geophys. Res. **100**(A9), 17,527–17,541, doi:10.1029/95JA01158.
Morozov, A. K., and Webb, D. C. (**2007**). "Underwater tunable organ-pipe sound source," J. Acoust. Soc. Am. **122**(2), 777–785.
National Research Council (NRC) (**2003**). "Ocean Noise and Marine Mammals" (National Academic Press, Washington, DC), pp. 83–108.
Nayar, K. G., Panchanathan, D., and McKinley, G. H. (**2014**). "Surface tension of seawater," J. Phys. Chem. Ref. Data **43**(4), 043103.
Norton, M. P., and Karczub, D. G. (**2003**). *Fundamentals of Noise and Vibration Analysis for Engineers* (Cambridge University Press, London).
Nowacek, D. P., Thorne, L. H., Johnston, D. W., and Tyack, P. L. (**2007**). "Responses of cetaceans to anthropogenic noise," Mammal Rev. **37**(2), 81–115.
Pécseli, H. L. (**2012**). *Waves and Oscillations in Plasmas* (CRC Press, Boca Raton, FL).
Plesset, M. S. (**1970**). "Effect of dissolved gases on cavitation in liquids (No. 85-55)," California Institute of Technology, Pasadena Division of Engineering and Applied Science.
Prosperetti, A., and Lezzi, A. (**1986**). "Bubble dynamics in a compressible liquid. Part 1. First-order theory," J. Fluid Mech. **168**, 457–478.
Rayleigh, O. M. (**1917**). "On the pressure developed in a liquid during the collapse of a spherical cavity," Philos. Mag. **34**(200), 94–98.
Reisman, G. E., Wang, Y. C., and Brennen, C. E. (**1998**). "Observations of shock waves in cloud cavitation," J. Fluid Mech. **355**, 255–283.
Richardson, W. J., Greene, C. R., Jr., Malme, C. I., and Thomson, D. H. (**1995**). *Marine Mammals and Noise* (Academic Press, New York), Chap. 1.
Russell, D., DuBois, D. F., and Rose, H. A. (**1986**). "Collapsing-caviton turbulence in one dimension," Phys. Rev. Lett. **56**(8), 838–841.
Southall, B. L., Bowles, A. E., Ellison, W. T., Finneran, J. J., Gentry, R. L., Greene, C. R., Jr., Kastak, D., Ketten, D. R., Miller, J. H., Nachtigall, P. E., and Richardson, W. J. (**2008**). "Marine mammal noise-exposure criteria: Initial scientific recommendations," Bioacoustics **17**(1–3), 273–275.
Spence, J. (**2009**). "Seismic survey noise under examination," Offshore **69**(5), 66–67.
Spence, J., Fischer, R., Bahtiarian, M., Boroditsky, L., Jones, N., Dempsey, R., and Life, M. (**2007**). "Review of existing and future potential treatments for reducing underwater sound from oil and gas industry activities," NCE Report, 07-001.
Versluis, M., Schmitz, B., von der Heydt, A., and Lohse, D. (**2000**). "How snapping shrimp snap: Through cavitating bubbles," Science **289**(5487), 2114–2117.
Wang, Y. C., and Brennen, C. E. (**1995**). "The noise generated by the collapse of a cloud of cavitation bubbles," in *American Society of Mechanical Engineers* (No. 226, pp. 17–29).
Weilgart, L. (**2013**). "A review of the impacts of seismic airgun surveys on marine life," submitted to the CBD Expert Workshop on Underwater Noise and its Impacts on Marine and Coastal Biodiversity, London, United Kingdom (February 25–27, 2014).

Williams, R., Clark, C. W., Ponirakis, D., and Ashe, E. (**2014**). "Acoustic quality of critical habitats for three threatened whale populations," Anim. Conserv. **17**, 174–185.
Woolf, D. K. (**2001**). "Bubbles," in *Encyclopedia of Ocean Sciences* (Academic Press, Cambridge, MA), pp. 352–357.
Wright, A. J., Soto, N. A., Baldwin, A. L., Bateson, M., Beale, C. M., Clark, C., Deak, T., Edwards, E. F., Fernández, A., Godinho, A., and Hatch, L. T. (**2007**). "Do marine mammals experience stress related to anthropogenic noise?," Int. J. Comp. Psychol. **20**(2), 247–316.
Yasui, K., Tuziuti, T., Lee, J., Kozuka, T., Towata, A., and Iida, Y. (**2010**). "Numerical simulations of acoustic cavitation noise with the temporal fluctuation in the number of bubbles," Ultrason. Sonochem. **17**(2), 460–472.
Ziolkowski, A. (**1970**). "A method for calculating the output pressure waveform from an air gun," Geophys. J. Int. **21**(2), 137–161.
Ziolkowski, A., Parkes, G., Hatton, L., and Haugland, T. (**1982**). "The signature of an air gun array: Computation from near-field measurements including interactions," Geophysics **47**(10), 1413–1421.